Following the Fate of Bacterial Cells Experiencing Sudden Chromosome Loss

Maya Elbaz, Sigal Ben-Yehuda

Department of Microbiology and Molecular Genetics, Institute for Medical Research Israel-Canada (IMRIC), The Hebrew University-Hadassah Medical School, The Hebrew University of Jerusalem, Jerusalem, Israel

ABSTRACT Chromosomal DNA is a constant source of information, essential for any given cell to respond and adapt to changing conditions. Here, we investigated the fate of exponentially growing bacterial cells experiencing a sudden and rapid loss of their entire chromosome. Utilizing *Bacillus subtilis* cells harboring an inducible copy of the endogenous toxin *yqcG*, which encodes an endonuclease, we induced the formation of a population of cells that lost their genetic information simultaneously. Surprisingly, these DNA-less cells, termed DLCs, did not lyse immediately and exhibited normal cellular morphology for a period of at least 5 h after DNA loss. This cellular integrity was manifested by their capacity to maintain an intact membrane and membrane potential and cell wall architecture similar to those of wild-type cells. Unlike growing cells that exhibit a dynamic profile of macromolecules, DLCs displayed steady protein and RNA reservoirs. Remarkably, following DLCs by time lapse microscopy revealed that they succeeded in synthesizing proteins, elongating, and dividing, apparently forming *de novo* Z rings at the midcell position. Taken together, the persistence of key cellular events in DLCs indicates that the information to carry out lengthy processes is harbored within the remaining molecular components.

IMPORTANCE Perturbing bacterial growth by the use of antibiotics targeting replication, transcription, or translation has been a subject of study for many years; however, the consequences of a more dramatic event, in which the entire bacterial chromosome is lost, have not been described. Here, we followed the fate of bacterial cells encountering an abrupt loss of their entire genome. Surprisingly, the cells preserved an intact envelope and functioning macromolecules. Furthermore, cells lacking their genome could still elongate and divide hours after the loss of DNA. Our data suggest that the information stored in the transient reservoir of macromolecules is sufficient to carry out complex and lengthy processes even in the absence of the chromosome. Based on our study, the formation of DNA-less bacteria could serve as a novel vaccination strategy, enabling an efficient induction of the immune system without the risk of bacterial propagation within the host.

Address correspondence to Sigal Ben-Yehuda, sigalb@ekmd.huji.ac.il.

DNA provides a living cell with the information required to grow, communicate, differentiate, survive, and die. The bacterial cell contains a centrally located large mass of chromosomal DNA (nucleoid), occupying the majority of its cytoplasmic space, and lacks a membrane-enclosed nucleus. The DNA is typically spread throughout the cell, such that the stored information is accessible for transcription into mRNA molecules that, in turn, are rapidly translated by ribosomes into proteins (1). Electron microscopy studies of bacterial chromosome structure provide evidence that transcription occurs on DNA loops. Based on these observations, it has been proposed that the transcription machinery and ribosomes are located in proximity within these loops, allowing coupled transcription and translation (2–7). Thus, the nucleoid seems to play a major role in facilitating orchestrated transcription and translation, serving not only as a template but also as a physical scaffold for these processes to occur simultaneously. The presence and the architecture of the chromosome as a scaffold is also underlined by its ability to constrain the subcellular distribution of macromolecules, such as ribosomes, and the divi-

sion machinery components (8–10). Spatial and temporal coordination of DNA accessibility, transcription, and translation is considered a requisite for optimal cellular functionality. This premise is supported by the cellular disarray observed upon disruption of replication, transcription, or translation by antibiotics (11). Nevertheless, protein and RNA synthesis have been shown to occur from plasmids in anucleated minicells, which are produced by misplaced septa in rod-shaped bacteria. Minicells, lacking subcellular organization, are unable to elongate and divide but still harbor some metabolic activities (12–17). However, the consequence of a more extreme circumstance, the abrupt loss of the entire bacterial chromosome in a population of exponentially growing cells, has not been described. Such a catastrophic event would prevent the cell from activating a regulated stress response, due to the absence of any genetic information, leaving the cell mainly with a transient reservoir of RNA and protein molecules. Additionally, such an event would perturb the global cellular architecture by causing the removal of a major cellular scaffold component.

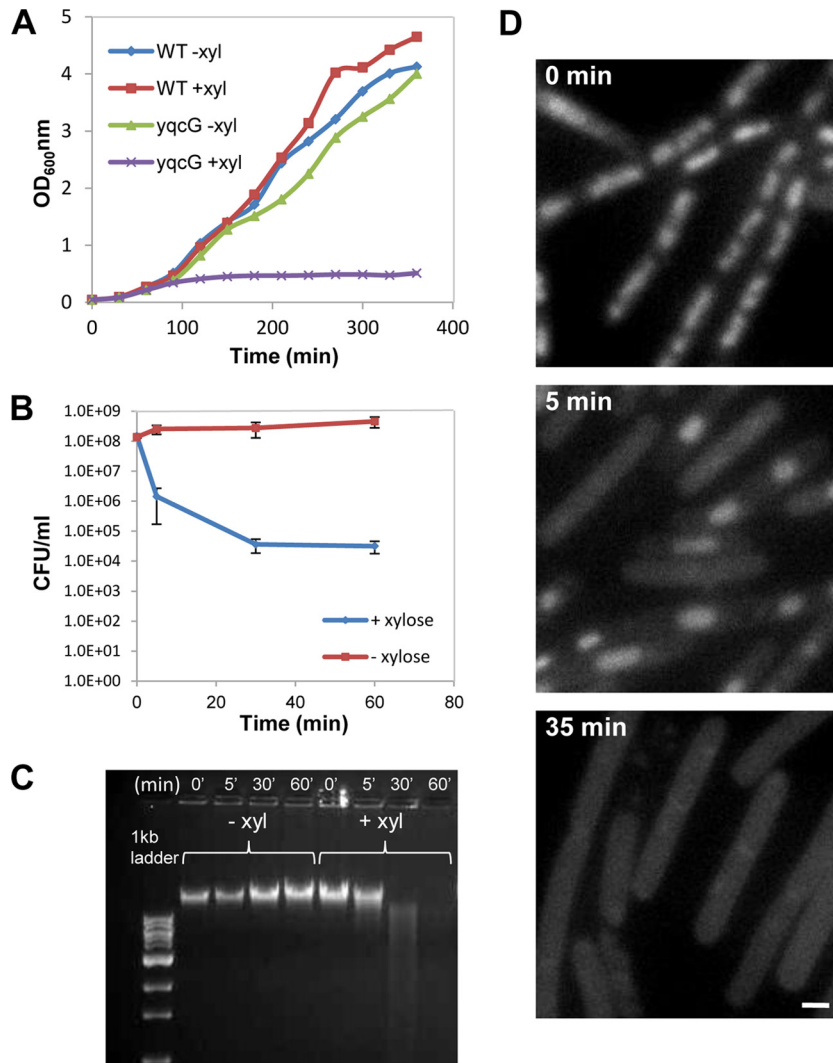To explore the fate of cells lacking DNA, we induced the deg-

FIG 1 YqcG degrades the DNA of growing *B. subtilis* cells. (A) Growth curves of wild-type (WT) (PY79) and P_{xyl}-*yqcG* Δ*yqcG* (ME187) strains grown at 37°C in LB medium with or without xylose as indicated. (B) CFU of P_{xyl}-*yqcG* Δ*yqcG* (ME187) cells grown at 37°C in LB medium with or without xylose were measured at the indicated time points. The time zero sample was plated before xylose addition. Shown are the averages of the normalized values from two independent biological repeats. Standard errors are indicated. (C) P_{xyl}-*yqcG* Δ*yqcG* (ME187) cells were grown at 37°C in LB medium with or without xylose, and genomic DNA was extracted at the indicated time points. The time zero sample was taken before xylose addition. The DNA concentration was determined using NanoDrop, and relatively similar amounts (approximately 50 μg DNA) were loaded onto 1% agarose gels. (D) Fluorescence images of P_{xyl}-*yqcG* Δ*yqcG* (ME187) cells grown at 37°C in LB medium with xylose and stained with DAPI were taken at the indicated time points. The time zero sample was visualized before xylose addition. Scale bar corresponds to 1 μm. Of note, sometimes residual DNA staining is observed by DAPI, usually in the vicinity of the membrane. This could be due to DNA fragments being protected from digestion by the membrane.

radation of the chromosome of growing *Bacillus subtilis* cells by activating an endonuclease. Remarkably, we found that, at least for a few hours, cells without DNA remain intact and are able to sustain homeostasis, as well as essential cellular activities. These findings reveal that complex cellular processes can progress in the absence of the nucleoid.

RESULTS

YqcG displays DNase activity. As part of our investigations into components that affect chromosome integrity and dynamics, we characterized the *yqcG*-*yqcF* toxin-antitoxin (TA) module (18). Our analysis revealed that the toxin component YqcG harbors robust endonuclease activity, as indicated by the following observations. In the absence of the antitoxin component, inserting *yqcG*

under a xylose-inducible promoter (P_{xyl}-*yqcG*) into *B. subtilis* cells resulted in rapid growth arrest and in a sharp decrease in CFU upon induction (Fig. 1A and B; see Fig. S1A in the supplemental material). The toxicity of *yqcG* was manifested by a massive decrease in CFU (99.98%), observed as early as 5 min postinduction (Fig. 1B). Furthermore, *yqcG*-induced cells exhibited rapid disappearance of the chromosome (Fig. 1C and D; see Fig. S1B): at approximately 30 min postinduction, the signal from 4′,6-diamidino-2-phenylindole (DAPI) staining was hardly detectable (out of ~2,000 cells that were visualized, none was found to exhibit chromosomal staining), and in accordance with this, DNA extracted from the cells was largely degraded. Consistent with these findings, when the chromosome was labeled with the DNA bind-

ing protein HBsu fused to green fluorescent protein (GFP), mislocalization of the fusion protein was evident subsequent to YqcG production (see Fig. S1C). A recent study reported that the *B. subtilis* YqcG C-terminal region acts as an RNase when expressed in *Escherichia coli* (18). However, we found no evidence for such activity when the full-length protein was expressed in *B. subtilis*, as the RNA remained intact for several hours after *yqcG* induction (see below). Taken together, our results indicate that YqcG possesses DNase activity when expressed in *B. subtilis*. This activity could therefore be utilized as a strategy to impose rapid chromosomal degradation. Henceforth, we term cells experiencing a sudden chromosome loss due to YqcG induction "DLCs," for DNA-less cells.

Following the integrity of DLCs. The capability to efficiently produce a synchronized DLC population prompted us to monitor the duration for which overall cellular integrity, activity, and biological functionalities could be preserved after such a deleterious event. As a first step in our investigation, we followed DLC morphology over time, using light microscopy. Surprisingly, DLCs clearly maintained their rod shape and membrane architecture, characteristics typical of wild-type cells, for at least 5 h after YqcG induction (Fig. 2A). Analyzing DLCs at later time points was complicated by the accumulation of suppressor cells, which harbored chromosomal DNA and dominated the culture. These suppressors arose from mutations within the C-terminal region of the *yqcG* open reading frame (see Fig. S1A in the supplemental material). To overcome this obstacle, we treated the DLC culture with the antibiotic nalidixic acid, which inhibits DNA gyrase and, therefore, should not affect DLCs, while eliminating the growth of suppressors. Remarkably, DLCs were found to be largely capable of maintaining their overall cellular morphology, even as long as 24 h after chromosome loss, though their membrane staining showed a nonhomogenous pattern, indicating some membrane perturbation (Fig. 2A).

To further examine the destiny of DLCs, we conducted a more detailed examination, focusing on the first 5 h after YqcG induction, when the population was composed solely of DLCs. We first asked whether DLCs that appear intact do indeed harbor a functional membrane. To address this question, DLCs were stained with propidium iodide (PI), which is incapable of penetrating intact membranes of living cells. Consistent with their morphological preservation, DLCs were impermeable to PI (see Fig. S2A in the supplemental material). As a control, when DLC membranes were artificially damaged by SDS treatment PI staining was visible (see Fig. S2B). In accordance with the sustained integrity of the membrane, membrane potential was preserved in DLCs, as indicated by their staining with the lipophilic fluorescent dye 3,3′-dihexyloxacarbocyanine iodide [$DiOC_6(3)$], which reports membrane functionality (Fig. 2B) (19, 20). Furthermore, as would be expected of wild-type cell membranes, $DiOC_6(3)$ staining was significantly reduced upon treating DLCs with the proton ionophore carbonyl cyanide *m*-chlorophenyl hydrazone (CCCP), which uncouples electron transport from ATP synthesis (Fig. 2B and C) (21). Assessment of metabolic activity using the MTT (3-[4,5-dimethylthiazol-2-yl]-2,5 diphenyl tetrazolium bromide) assay, which monitors the reduction of MTT by NAD(P)H-dependent cellular oxidoreductases, showed that DLCs maintained metabolic activity at approximately half of the level exhibited by the cells before YqcG induction (Fig. 2D).

We have previously shown an intimate connection between cell wall integrity and chromosome organization and segregation,

demonstrating that direct perturbation of the cell wall leads to polyploid cells with atypical nucleoid morphologies (22). DLCs offered the opportunity to ask if the link between chromosome structure and cell wall integrity is reciprocal. Since DLCs maintain the rod shape structure, we attempted to elucidate whether their cell wall is intact. To examine the DLC peptidoglycan (PG) structure, cells were labeled with fluorescent wheat germ agglutinin (WGA), which demarcates the cell wall (23, 24). Consistent with preservation of their membrane integrity, DLCs displayed typical bright midcell bands and helical sidewall staining similar to those of normal cells (see Fig. S3 in the supplemental material). Thus, it appears that the presence of the chromosome does not dictate the PG structure. Moreover, once the cell wall is formed, genetic information is not essential for its maintenance for at least 5 h after chromosome loss.

Taken together, our data imply that DLCs remain intact for several hours after experiencing chromosome loss, as manifested by a proper overall cell shape, a membrane that operates as a selective barrier, and a normal PG pattern. These findings suggest that DLCs are not halted in an inactive mode but, instead, seem capable of maintaining basic cellular activities. Thus, although DLCs are no longer alive according to classical definitions, their viability measurements are similar to those of wild-type cells.

Macromolecules are preserved and remain functional in DLCs. A living cell exhibits dynamic coordination between the key cellular processes of replication, transcription, and translation. DLCs afford tracking of RNA and protein molecules when this synchrony is perturbed by chromosome loss. Intriguingly, RNA extracted from DLCs possessed a profile similar to that of normal cells, showing only slight degradation in the course of 5 h after genome loss (Fig. 3A). In line with the RNA stability observed in DLCs, Bradford and SDS-PAGE analyses of total protein content showed no apparent differences in the overall protein concentration, nor did they show obvious changes in the pattern of protein bands over time (Fig. 3B). Following both the DNA and protein concentrations extracted from the same cultures over time substantiated that the protein concentration remained stable, while the DNA level was reduced (see Fig. S4A in the supplemental material). We next examined in detail the stability of specific proteins with diverse cellular functions: RplA, a ribosomal subunit (25, 26), Spo0J, a DNA binding protein involved in chromosome segregation (27–29), ManP, a membrane transporter of mannose (30), and FtsZ, the major cell division protein (31, 32). To this end, DLCs harboring GFP fusions to each of the representative proteins were subjected to Western blot analysis. In parallel, the level of the housekeeping protein sigma factor A (33, 34) was determined for each of the examined strains as a control. A relatively constant protein level was observed over time for all of the proteins inspected (see Fig. S4B), corroborating the overall lack of significant change in total protein concentration. Accordingly, the intensity of the fluorescent signal deriving from DLCs harboring RplA-GFP or ManP-GFP was relatively steady (see Fig. S4C and D). Based on these observations, we conclude that cells that have lost their genome in a sudden and rapid manner preserve macromolecules in a stable state.

The observed protein stability could reflect steady-state dynamics or, alternatively, a pause during which the cell is lacking in protein synthesis and degradation. To address this issue, we conducted a fluorescence recovery after photobleaching (FRAP) assay, monitoring DLCs expressing RplA-GFP. Following photo-
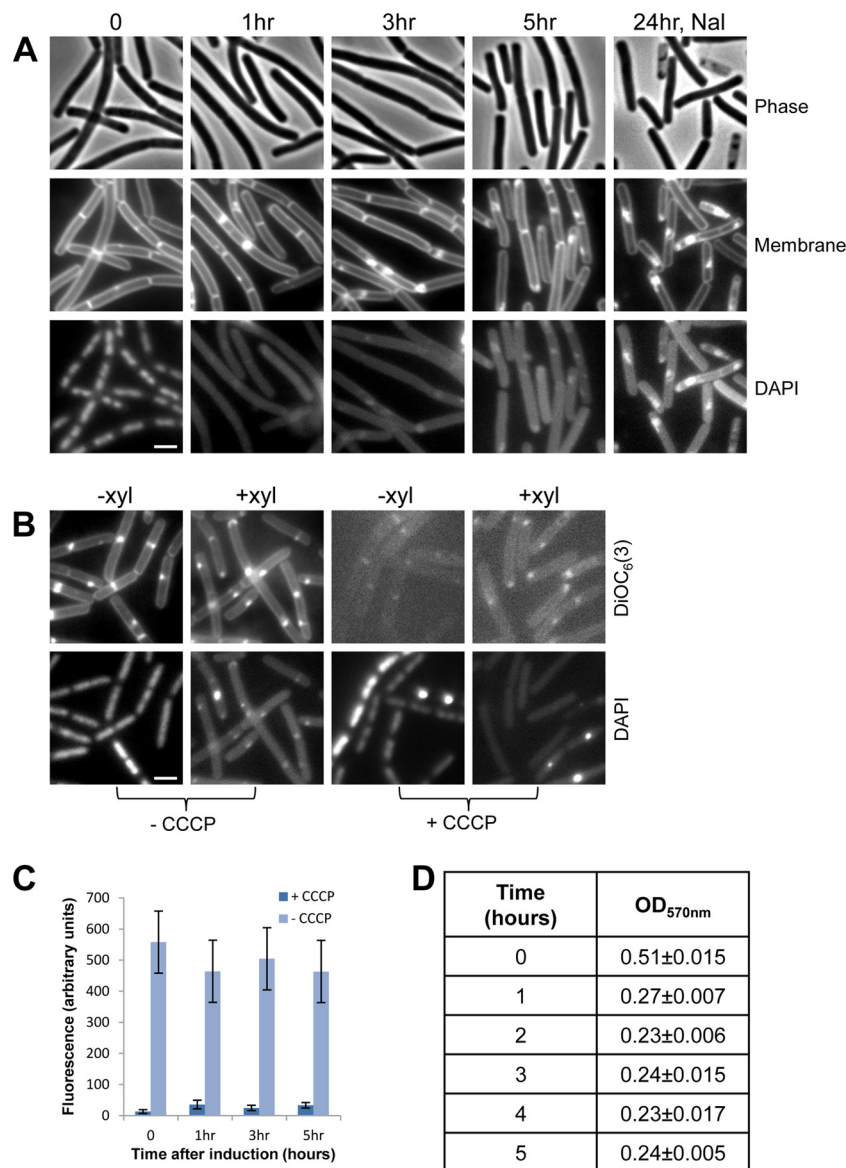
FIG 2 DLCs maintain cellular integrity. (A) Phase contrast, membrane staining, and DAPI images of P_{xyl}-$yqcG$ $\Delta yqcG$ (ME187) cells grown at 37°C in LB medium with xylose at the indicated time points. The time zero sample was visualized before xylose addition. Nalidixic acid (Nal; 500 μg/ml) was added 5 h postinduction. Scale bar corresponds to 2 μm. Of note, the DAPI signal in DLCs is likely to emanate from leakage of the membrane dye. (B) P_{xyl}-$yqcG$ $\Delta yqcG$ (ME187) cells were grown at 37°C in LB medium with or without xylose, as indicated. After 1 h of incubation, samples were treated with CCCP as indicated. Samples were stained with $DiOC_6(3)$ and DAPI and visualized by fluorescence microscopy. Scale bar corresponds to 2 μm. (C) P_{xyl}-$yqcG$ $\Delta yqcG$ (ME187) cells were grown at 37°C in LB medium, and samples taken before ($t = 0$) and after ($t = 1$, 3, or 5 h) xylose addition were treated with CCCP, as indicated. Samples were stained with $DiOC_6(3)$ and visualized by fluorescence microscopy. Shown are the results for quantification of the fluorescence signal from $DiOC_6(3)$-treated samples. For each time point, 200 cells were analyzed. Standard deviations (SD) are indicated. (D) P_{xyl}-$yqcG$ $\Delta yqcG$ (ME187) cells were grown at 37°C in LB medium, and samples taken before ($t = 0$) and after ($t = 1$ to 5 h) xylose addition were incubated with MTT reagent (0.4 mg/ml) for 2 h. The resulting purple formazan was solubilized by SDS and quantified by spectrophotometry at 570 nm. The values presented, measured from 6×10^7 cells, are the average results from triplicates. SD are indicated.

bleached DLCs by time lapse microscopy revealed recovery of the signal, though with slow kinetics (26), as evidenced by the increase in fluorescence 1 to 2 h post-bleaching (Fig. 3C; see Fig. S5A in the supplemental material). Importantly, this increase was inhibited when FRAP was conducted in the presence of chloramphenicol (see Fig. S5B and C). Evaluation of protein synthesis by measuring [35S]methionine incorporation indicated that, indeed, DLCs continue to produce proteins with slower kinetics than cells prior to DNA degradation (Fig. 3D).

Thus, DLCs contain RNA molecules that are accessible for translation, as well as functional ribosomes that are capable of protein production. These features suggest that DLCs are most likely kept in a steady-state dynamic mode.

Protein localization within DLCs. Having established that proteins are preserved within DLCs, we examined the localization of the representative GFP fusion proteins before and after chromosome loss. Notably, a shift in RplA-GFP localization from the typical condensed polar foci to a cytoplasmic diffusible pattern
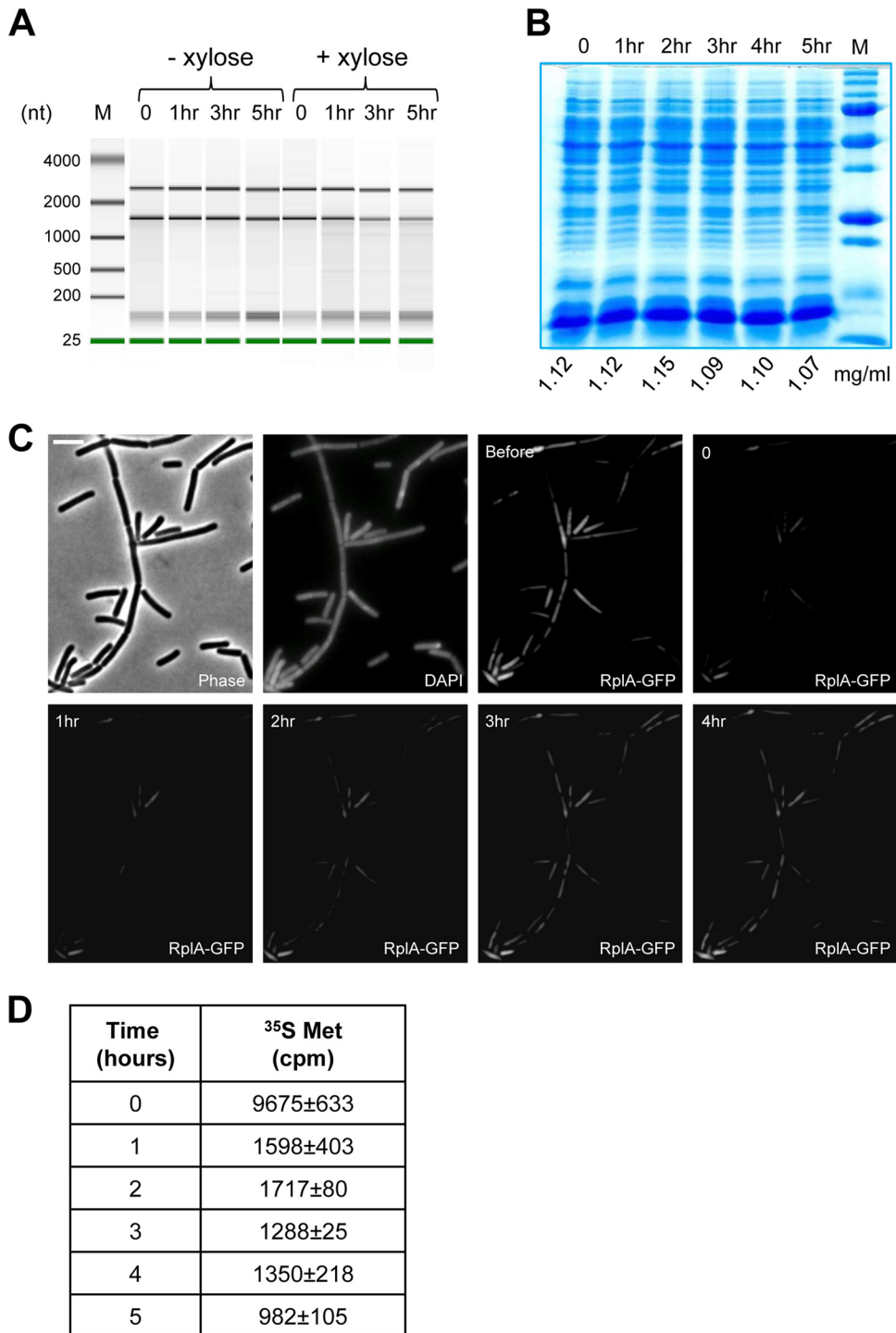
FIG 3 Macromolecules remain steady and functional in DLCs. (A) Bioanalyzer pseudogel of RNA extracted from P_{xyl}-$yqcG$ $\Delta yqcG$ (ME187) cells grown at 37°C in LB medium with or without xylose at the indicated time points. The time zero sample was taken before xylose addition. All lanes in the pseudogel are scaled to the same intensity range. M, molecular size ladder. (B) SDS-PAGE of proteins extracted from P_{xyl}-$yqcG$ $\Delta yqcG$ (ME187) cells grown at 37°C in LB medium before ($t = 0$) and after ($t = 1$ to 5 h) xylose addition. Protein concentrations were determined by Bradford assay and are indicated below the lanes. (C) Xylose was added to growing P_{xyl}-$yqcG$ $\Delta yqcG$ cells harboring $rplA$-gfp (ME260). After 1 h, cells were incubated at 37°C on an LB agarose pad containing xylose and subjected to FRAP analysis. Shown are phase contrast, DAPI, and RplA-GFP fluorescence images. Time points before (Before) and after (0 to 4 h) photobleaching are indicated. Scale bar corresponds to 4 μm. (D) P_{xyl}-$yqcG$ $\Delta yqcG$ (ME187) cells were grown at 37°C in LB medium, and samples taken before ($t = 0$) and after ($t = 1$ to 5 h) xylose addition were incubated with [^{35}S]methionine (^{35}S Met) for 30 min at 37°C. The radioactivity values presented (counts per minute [cpm]), measured from 1×10^7 cells, are the average results of triplicates. SD are indicated. Notably, the experiment was carried out in LB medium, since YqcG degradation activity is less efficient when cells are grown in minimal medium. Therefore, the values obtained for [^{35}S]methionine incorporation are probably an underestimation, as unlabeled methionine was present in the medium.
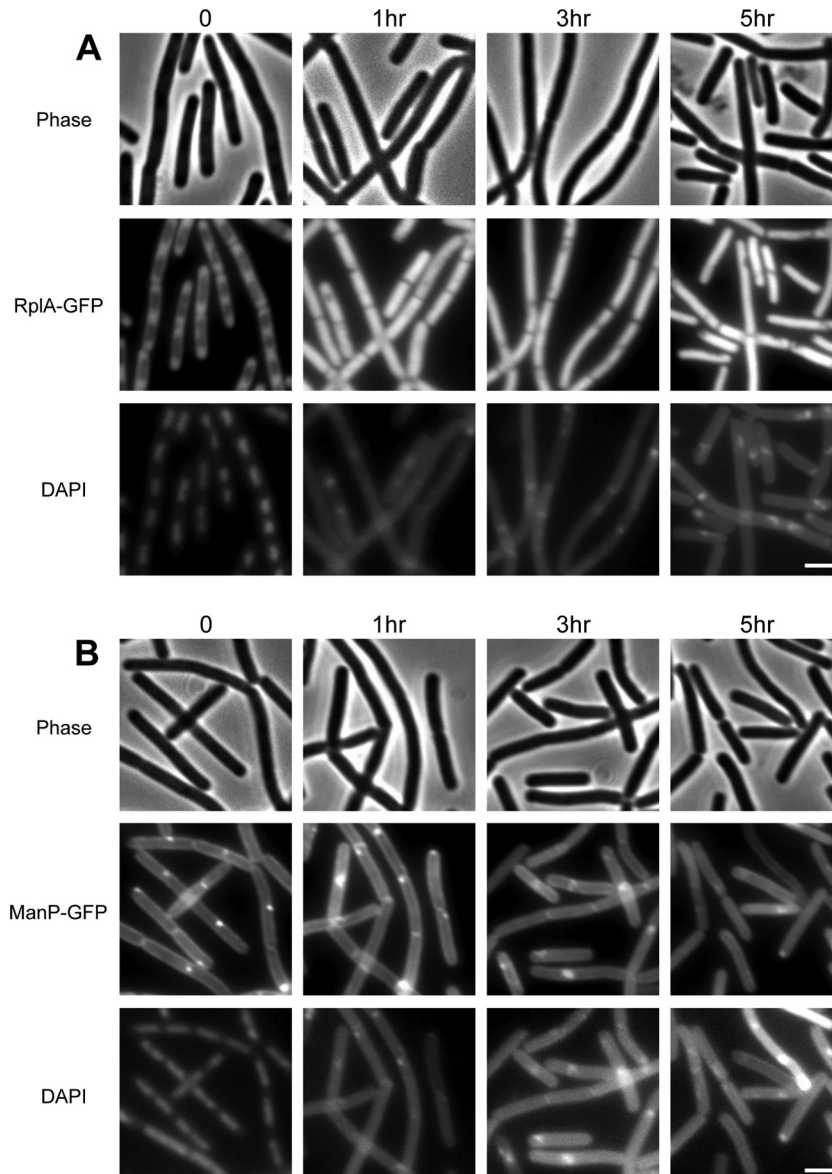
FIG 4 Expression and localization patterns of RplA and ManP in DLCs. (A and B) Phase contrast and fluorescence images of P_{xyl}-$yqcG$ $\Delta yqcG$ cells harboring $rplA$-gfp (ME260) (A) and P_{xyl}-$yqcG$ $\Delta yqcG$ cells harboring $manP$-gfp (ME249) (B); cells were grown at 37°C in LB medium with xylose and stained with DAPI at the indicated time points. The time zero sample was visualized before xylose addition. Scale bars correspond to 2 μm.

was observed following DNA degradation (Fig. 4A). This change in localization could be driven by the liberation of the ribosomes from their confined cellular zone, which is normally dictated by the chromosomal mass (9). Spo0J-GFP, which binds to the $oriC$ region (27, 29, 35, 36), became more diffusely localized concomitantly with the process of DNA degradation (see Fig. S6 in the supplemental material), as might be expected. Unlike RplA and Spo0J, the localization of the mannose transporter ManP was largely preserved for at least 5 h after YqcG induction (Fig. 4B), reinforcing the view that the cytoplasmic membrane of DLCs remains functional throughout this time. In line with the premise of sustained functionality, approximately 40% of the DLCs contained FtsZ rings (Z rings), in comparison to ~60% of the cells before YqcG induction (see Fig. S7A and B). Notably, around 5% of the DLC Z rings appeared as extended helical structures, while

only 1% of the Z rings displayed such pattern prior to YqcG induction. Measuring the Z ring position within DLCs revealed that the majority were properly localized to sites of division in the vicinity of the midcell; however, a slight shift from their customary central position was detected (see Fig. S7C). This typical localization pattern of FtsZ was largely maintained throughout the course of the experiment, raising the possibility that Z ring positioning is independent of the physical presence of the nucleoid. Furthermore, the correct localization of Z rings in DLCs suggests that the division machinery could still operate despite the absence of the chromosome.

DLCs can elongate and divide. So far, we have shown that DLCs preserve their cellular morphology, contain an intact membrane and stable macromolecules, and exhibit proper localization of the cell division initiator protein FtsZ. These observations raise
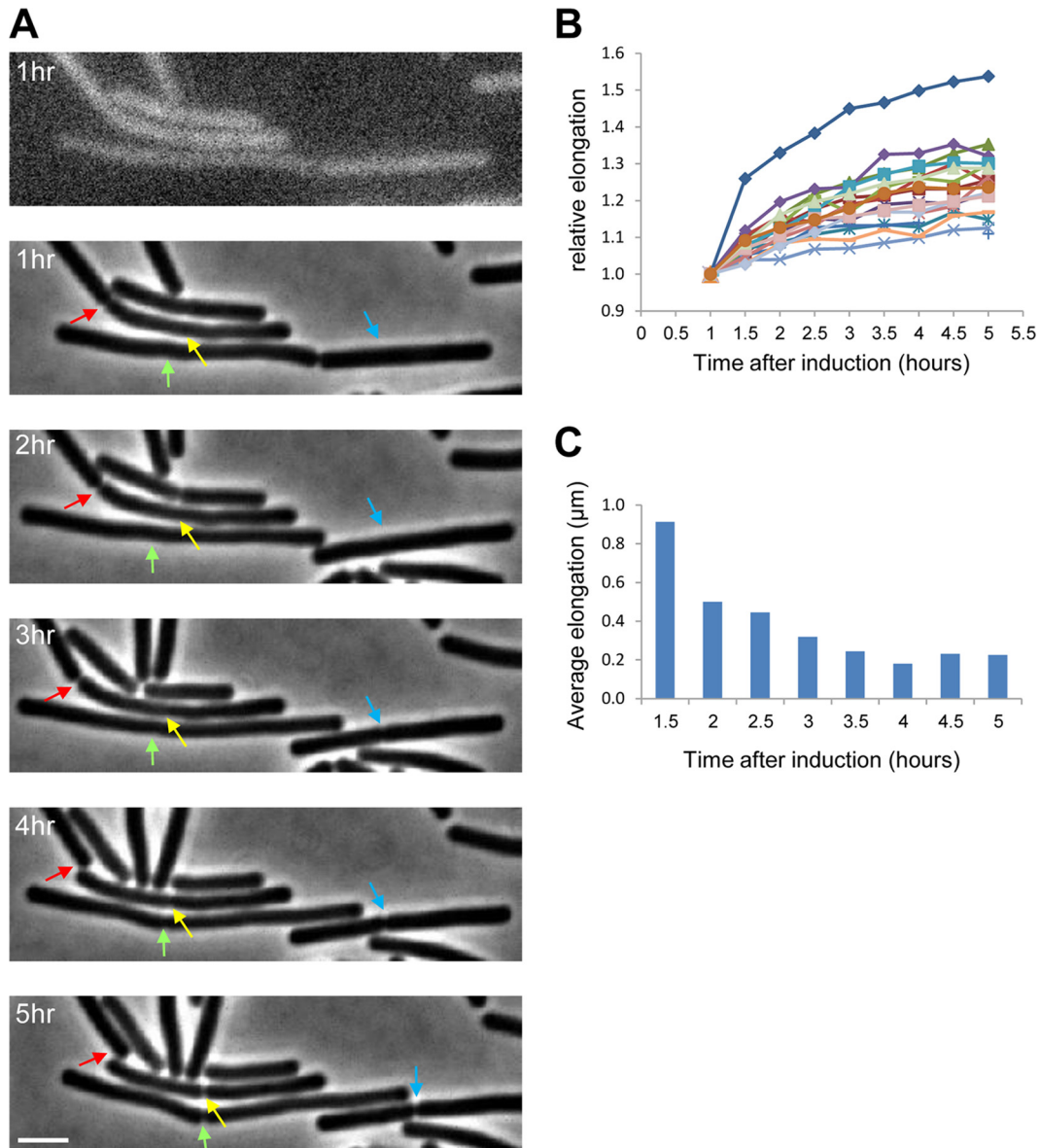
FIG 5 DLCs elongate and divide. (A) P_{xyl}-$yqcG$ $\Delta yqcG$ cells harboring $hbsu$-gfp (ME233) were grown at 37°C on an LB agarose pad containing xylose and were followed by time lapse microscopy. The top panel shows the signal from HBsu-GFP, indicating DNA loss (see Fig. S1C). The subsequent panels show phase contrast images taken at the indicated time points. Arrows highlight positions of division sites. Each color signifies a given site over time. Scale bar corresponds to 2 μm. (B) Elongation of individual ME233 DLCs was followed by time lapse microscopy. Shown are the relative lengths over time of 20 individual cells for which the length at the 1-h time point was defined as 1. The average elongation of ME233 cells grown without xylose (harboring intact chromosomes) under the same conditions was ×1.5 per 30 min, as calculated from 50 individual cells. (C) The average results for ME233 cell elongation over time were extracted from the data shown in panel B.

the question of whether FtsZ can provide a platform to carry out the fundamental process of cell division in the absence of DNA or whether Z rings are halted in a nondynamic state. To address this question, we followed DLCs by time lapse microscopy. Remarkably, we could clearly observe DLCs elongating and eventually separating into individual cells, implying that their Z rings are functional and can facilitate cell division (Fig. 5A). Following the elongation of individual DLCs revealed the elongation rate to be the highest during the initial 2.5 h after DNA loss and to subsequently decrease (Fig. 5B and C). We then attempted to explore whether the observed Z rings

are only formed prior to chromosome loss or could also be established *de novo*. Tracking FtsZ-GFP within DLCs by time lapse microscopy showed that even after DNA loss, FtsZ forms dynamic rings that can undergo assembly and constriction (Fig. 6A and B). Following the Z ring dynamics using FRAP assay revealed that existing rings can successfully recruit new FtsZ molecules (Fig. 6C). Furthermore, the FRAP analysis evidenced that DLCs are capable of forming *de novo* Z rings (Fig. 6D). The appearance of *de novo* Z rings in DLCs was approximately 8.5% of the total Z rings and persisted even 5 h after YqcG induction (Fig. 6E). Collectively, these findings sug-
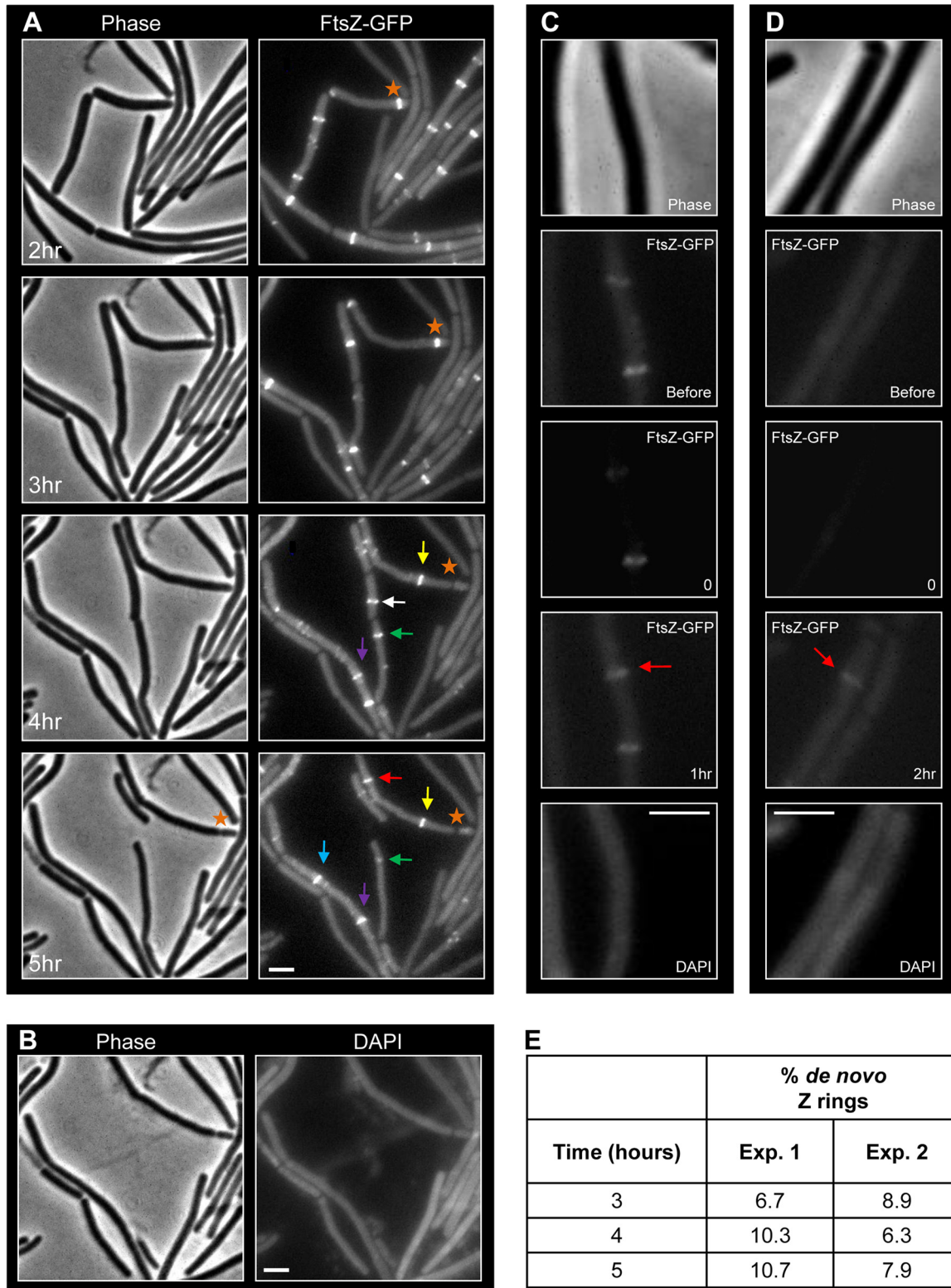
FIG 6 Z ring dynamics in DLCs. (A) P_{xyl}-$yqcG$ $\Delta yqcG$ cells harboring $ftsZ$-gfp (ME244) were grown at 30°C on an LB agarose pad containing xylose and were followed by time lapse microscopy. Phase contrast and FtsZ-GFP fluorescence images were taken at the indicated time points. Arrows highlight positions of *de novo* Z rings, and stars indicate a constricting Z ring leading to cell division. Each color arrow signifies a given Z ring over time. (B) As a complement to the experiment whose results are shown in panel A, DAPI staining, which is toxic to cells, was added at the latest time point ($t = 5$ h); the results indicate the absence of chromosomal DNA. Of note, the position of some of the cells within the image changed following DAPI addition. (C and D) Xylose was added to growing P_{xyl}-$yqcG$ $\Delta yqcG$ cells harboring $ftsZ$-gfp (ME244). After 2.5 h, the cells were incubated at 30°C on an LB agarose pad containing xylose and subjected to FRAP analysis. Phase contrast, FtsZ-GFP fluorescence, and DAPI images show recruitment of FtsZ molecules to an existing ring (arrow) (C) or *de novo* Z ring formation

(Continued)

gest that cell division in DLCs is a regulated process rather than spontaneous polymerization and constriction of Z rings.

DISCUSSION

Chromosome integrity is considered fundamental for the maintenance of any functional cell, with even point mutations being sufficient to trigger cell death and lysis. Here, we investigated the fate of bacterial cells which have lost their entire nucleoid in a sudden and rapid fashion. Surprisingly, DLCs maintained an intact membrane, as well as the characteristic architecture of the cell wall. In addition, DLCs successfully preserved their macromolecules, as indicated by steady RNA and protein levels for a period of at least 5 h. Furthermore, DLCs were not arrested in an inactive mode but could synthesize proteins, elongate, accurately position new Z rings, and divide. Thus, the continuity of key cellular events in cells lacking their chromosome indicates that the cues to carry out complex and lengthy processes are harbored within downstream molecular components.

The chromosome constitutes a physical scaffold that enables simultaneous transcription and translation (2–7) and influences protein localization. In accordance with this structural role, ribosomes were found to be excluded from the nucleoid-occupied regions, localizing mainly to the cell poles and the chromosome periphery (9). Consistent with this view, the ribosomal subunit RplA was observed to become diffusible in DLCs. Alternatively, RplA mislocalization could emanate from the lack of transcription, which has been shown to affect ribosome subcellular positioning (37). A profound effect of the physical presence of the nucleoid is to constrain the localization of the division machinery. It has been demonstrated that chromosome-associated proteins act to directly inhibit the assembly of the division apparatus around the nucleoid (8, 10). While Z ring assembly in cells devoid of DNA could potentially occur all over the cell, Z rings seem to be localized mainly to the midcell in DLCs, though some increase in Z rings displaying helical structures was monitored. This observation is consistent with previous studies showing that Z rings are positioned at the midcell in nucleoid-free *E. coli* cells formed in response to UV irradiation or derived from *parC* and *mukB* mutants and in cells lacking the nucleoid occlusion system (38–41). Although the FtsZ protein was shown to harbor intrinsic properties to assemble into multiple rings in liposomes and generate force for constriction (42), in general, a single Z ring per cell was exhibited by DLCs, suggesting that this phenomenon is not due to random polymerization. Furthermore, following cell elongation, DLCs were frequently capable of completing cell division, implying that the division machinery was functioning properly.

Macromolecule turnover is vital in bacteria to facilitate rapid responses to changing environments and for developmental processes to take place (43–46). Unexpectedly, RNA and protein levels were found to be relatively stable within DLCs, showing slow protein synthesis kinetics. These findings suggest that synthesis and degradation are carried out in DLCs, albeit on a longer time scale than in wild-type cells. Possibly, this slower kinetics is due to a lack of the energy required to facilitate molecular synthesis and

degradation, along with the physical lack of a template for new RNA synthesis. Consistent with these possibilities, DLC elongation and division capabilities are energy-consuming processes occurring more slowly than normal. It is conceivable that DLCs are committed to perform particular cellular tasks and harbor energy reservoirs to fuel their occurrence. In light of this notion, normal cells might reserve energy pools to ensure the progression and completion of ongoing pathways.

Although an active apoptotic death pathway has mainly been attributed to eukaryotic cells, accumulating evidence indicates that similar destruction events exist in bacteria (47). Indeed, bacterial cells were shown to activate a regulated stress response, such as SOS or programmed cell death (PCD), following toxin activation, DNA damage, or exposure to antibiotics (48–51). Under such circumstances, morphological and biochemical hallmarks of apoptosis, including DNA fragmentation and membrane depolarization, have been observed in bacterial cells. Since cells lacking a chromosome cannot respond to stress conditions by activating the corresponding set of genes, the maintenance of DLC integrity hours after DNA degradation reinforces the view that active cell death is an attribute of bacteria. Consistent with this model, DNA topoisomerase-targeting antibiotics require protein synthesis to induce death (11, 52). Taken together, bacterial cell death could be an intrinsic apoptotic regulated pathway, demanding gene activation for its accomplishment. DLCs, being unable to induce a stress response, sustain cellular processes without being able to execute active cell death.

Cellular genetic information is generally considered a prerequisite for the performance of complex and prolonged processes. However, evidence for the occurrence of fundamental cellular processes, such as protein synthesis, division, and PCD, was observed in anucleated platelets in mammalians (53). Nevertheless, in contrast to DLCs, chromosome loss in platelets is programmed, taking place in cells destined for such an event. Platelets and DLCs both exemplify the notion that, once the information flows from the DNA to downstream components, the latter become independent, capable of carrying out fundamental processes to sustain cellular existence. Interestingly, studies of minicells, conducted mainly in the 1970s, indicate that they are capable of performing respiration, incorporating amino acids into their cell wall, and synthesizing proteins and RNA from phages and plasmids (12–17).

Despite considerable attempts, we failed to reveal the actual physiological role of the *yqcGF* TA module. Conducting an array of experiments, such as competition assays between wild-type and Δ*yqcGF* mutant cells and testing the effects of Δ*yqcGF* mutation on competence, sporulation, DNA repair, and phage infection, did not expose any detectable phenotype. However, the DLC characterization provided here can serve as a platform for future investigation of specific molecular processes, such as PCD. In this regard, DLCs can also be utilized as recipients for transplantation of synthetic DNA (54). The ability of DLCs to perform sophisticated cellular activities brings about the possibility of utilizing a similar approach for pathogenic bacteria as a potential vaccina-

Figure Legend Continued

(arrow) (D). Time points before (before) and after (1 h or 2 h) photobleaching are indicated. Scale bars correspond to 2 μm. (E) ME244 cells were followed by time lapse microscopy as described for panel A, and the percentages of *de novo* Z rings out of the total Z rings for each time point after YqcG induction were calculated. At least 215 Z rings were scored for each time point. Shown are results from two independent biological experiments (Exp.).

tion strategy. DLCs are likely to be capable of efficiently inducing the immune system without propagating within the host.

MATERIALS AND METHODS

Strains and general methods. *B. subtilis* strains are listed in Table S1 in the supplemental material. The plasmid and primers used for this study are described in Text S1 and Table S2. All general methods were carried out as described previously (55). Cultures were inoculated at an optical density at 600 nm (OD_{600}) of 0.05 from an overnight culture, and growth was carried out at 30°C or 37°C in LB medium. During logarithmic phase (OD_{600} of 0.4 to 0.6), 0.5% xylose was added to induce *yqcG* expression, as indicated. Of note, induction of YqcG during stationary phase or in minimal medium does not lead to efficient DNA degradation, suggesting that under these conditions, the chromosome is protected from YqcG endonuclease activity.

Fluorescence microscopy. Fluorescence microscopy was carried out as described previously (22). Briefly, samples (0.5 ml) were taken during logarithmic phase, centrifuged, and resuspended in 10 μl of 1× phosphate-buffered saline (PBS) supplemented with the fluorescent membrane stain FM1-43 (Molecular Probes; Invitrogen) at 1 μg/ml and/or with the DNA stain 4,6-diamidino-2-phenylindole (DAPI) (Sigma) at 2 μg/ml. For cell wall labeling, cells were harvested, gently centrifuged, resuspended in 100 μl 1× T-Base supplemented with wheat germ agglutinin (WGA)-fluorescein isothiocyanate (FITC) (5 μg/ml; Sigma), incubated for 15 min at room temperature, and washed twice with 1× T-Base before imaging. To visualize stained cell walls and GFP-fused proteins, the cells were placed on thin 1× T-Base–1% agarose pads. For SDS treatment, cells (0.5 ml) were incubated with 0.06% SDS for 10 min at room temperature, washed twice with 1× PBS, and stained with DAPI and propidium iodide (PI) (5 μg/ml; Sigma) before imaging. Cells were visualized and photographed using an Axioplan2 microscope (Zeiss) equipped with a CoolSnap HQ camera (Photometrics, Roper Scientific) or an Axio Observer Z1 microscope (Zeiss) equipped with a CoolSnap HQII camera (Photometrics; Roper Scientific). System control and image processing were performed using MetaMorph software (Molecular Devices).

Assessing membrane potential. To assess membrane potential, cells were grown to logarithmic phase and samples (1 ml) were harvested. Cells were washed once with 1× PBS and incubated for 1 min with 10 nM $DiOC_6(3)$ (Invitrogen) diluted in 1× PBS. As a control, before $DiOC_6(3)$ staining, cells were incubated with 100 μM CCCP for 5 min. Cells were visualized and photographed by fluorescence microscopy, and signal intensities were evaluated using MetaMorph software (Molecular Devices).

MTT assay. For estimating cell metabolic activity, the MTT assay was conducted as previously described (56). In brief, cells were grown to logarithmic phase and samples were diluted (1:16, within the linear range) in 1 ml LB medium. MTT reagent was added to a final concentration of 0.4 mg/ml, and samples were incubated at 37°C for 2 h. For dissolving formazan, 100 μl of 10% SDS was added. The level of formazan was measured by spectrophotometer (OD_{570}). A sample of LB medium supplemented with MTT reagent and SDS served as a control.

Pulse and chase [^{35}S]methionine labeling. For monitoring protein synthesis, cells were grown to logarithmic phase, and samples (400 μl) were incubated with [^{35}S]methionine (24 μCi) at 37°C for 30 min. Ten microliters of a given sample was then spotted in triplicates onto 3MM Whatman paper. The dried filters were incubated in cold 10% 2,4,6-trichloroanisole (TCA) for 30 min, washed with cold 10% TCA for 15 min, and finally left in fresh 10% TCA overnight at 4°C. Next, samples were washed with cold 95% ethanol and left to dry. Radioactivity was determined by scintillation counter (Tri-Carb 2900 TR; Packard). Samples of LB medium supplemented with [^{35}S]methionine and samples of cells incubated in the absence of [^{35}S]methionine served as controls.

For additional methods, see Text S1 in the supplemental material.

SUPPLEMENTAL MATERIAL

ACKNOWLEDGMENTS

REFERENCES

1. **Lodish HF, Berk A, Krieger M, Kaiser CA, Scott MP, Bretscher A, Polegh H, Matsudaria P.** 2008. Molecular cell biology, 6th ed. W. H. Freeman, Basingstoke, United Kingdom.
2. **Hobot JA, Villiger W, Escaig J, Maeder M, Ryter A, Kellenberger E.** 1985. Shape and fine structure of nucleoids observed on sections of ultra-rapidly frozen and cryosubstituted bacteria. J Bacteriol **162:**960–971.
3. **Miller OL, Jr., Hamkalo BA, Thomas CA, Jr.** 1970. Visualization of bacterial genes in action. Science **169:**392–395. http://dx.doi.org/10.1126/science.169.3943.392.
4. **Robinow C, Kellenberger E.** 1994. The bacterial nucleoid revisited. Microbiol Rev **58:**211–232.
5. **Ryter A, Chang A.** 1975. Localization of transcribing genes in the bacterial cell by means of high resolution autoradiography. J Mol Biol **98:**797–810. http://dx.doi.org/10.1016/S0022-2836(75)80011-8.
6. **Valkenburg JA, Woldring CL, Brakenhoff GJ, van der Voort HT, Nanninga N.** 1985. Confocal scanning light microscopy of the *Escherichia coli* nucleoid: comparison with phase-contrast and electron microscope images. J Bacteriol **161:**478–483.
7. **Woldringh CL, Jensen PR, Westerhoff HV.** 1995. Structure and partitioning of bacterial DNA: determined by a balance of compaction and expansion forces? FEMS Microbiol Lett **131:**235–242. http://dx.doi.org/10.1111/j.1574-6968.1995.tb07782.x.
8. **Bernhardt TG, de Boer PA.** 2005. SlmA, a nucleoid-associated, FtsZ binding protein required for blocking septal ring assembly over chromosomes in *E. coli*. Mol Cell **18:**555–564. http://dx.doi.org/10.1016/j.molcel.2005.04.012.
9. **Lewis PJ, Thaker SD, Errington J.** 2000. Compartmentalization of transcription and translation in *Bacillus subtilis*. EMBO J **19:**710–718. http://dx.doi.org/10.1093/emboj/19.4.710.
10. **Wu LJ, Errington J.** 2004. Coordination of cell division and chromosome segregation by a nucleoid occlusion protein in *Bacillus subtilis*. Cell **117:**915–925. http://dx.doi.org/10.1016/j.cell.2004.06.002.
11. **Kohanski MA, Dwyer DJ, Collins JJ.** 2010. How antibiotics kill bacteria: from targets to networks. Nat Rev Microbiol **8:**423–435. http://dx.doi.org/10.1038/nrmicro2333.
12. **Adler HI, Fisher WD, Cohen A, Hardigree AA.** 1967. Miniature *Escherichia coli* cells deficient in DNA. Proc Natl Acad Sci U S A **57:**321–326. http://dx.doi.org/10.1073/pnas.57.2.321.
13. **Mendelson NH, Reeve JN, Cole RM.** 1974. Physiological studies of *Bacillus subtilis* minicells. J Bacteriol **117:**1312–1319.

14. **Mertens G, Reeve JN**. 1977. Synthesis of cell envelope components by anucleate cells (minicells) of *Bacillus subtilis*. J Bacteriol **129:**1198–1207.

15. **Reeve JN, Cornett JB**. 1975. Bacteriophage SPO1-induced macromolecular synthesis in minicells of *Bacillus subtilis*. J Virol **15:**1308–1316.

16. **Reeve JN, Mendelson NH, Coyne SI, Hallock LL, Cole RM**. 1973. Minicells of *Bacillus subtilis*. J Bacteriol **114:**860–873.

17. **Roozen KJ, Fenwick RG, Jr, Curtiss R, III**. 1971. Synthesis of ribonucleic acid and protein in plasmid-containing minicells of *Escherichia coli* K-12. J Bacteriol **107:**21–33.

18. **Holberger LE, Garza-Sánchez F, Lamoureux J, Low DA, Hayes CS**. 2012. A novel family of toxin/antitoxin proteins in *Bacillus* species. FEBS Lett **586:**132–136. http://dx.doi.org/10.1016/j.febslet.2011.12.020.

19. **Laflamme C, Ho J, Veillette M, de Latrémoille MC, Verreault D, Mériaux A, Duchaine C**. 2005. Flow cytometry analysis of germinating *Bacillus* spores, using membrane potential dye. Arch Microbiol **183:**107–112. http://dx.doi.org/10.1007/s00203-004-0750-9.

20. **Sträuber H, Müller S**. 2010. Viability states of bacteria-specific mechanisms of selected probes. Cytometry A **77:**623–634. http://dx.doi.org/10.1002/cyto.a.20920.

21. **Ghoul M, Pommepuy M, Moillo-Batt A, Cormier M**. 1989. Effect of carbonyl cyanide m-chlorophenylhydrazone on *Escherichia coli* halotolerance. Appl Environ Microbiol **55:**1040–1043.

22. **Elbaz M, Ben-Yehuda S**. 2010. The metabolic enzyme ManA reveals a link between cell wall integrity and chromosome morphology. PLoS Genet **6:**e1001119. http://dx.doi.org/10.1371/journal.pgen.1001119.

23. **Hayhurst EJ, Kailas L, Hobbs JK, Foster SJ**. 2008. Cell wall peptidoglycan architecture in *Bacillus subtilis*. Proc Natl Acad Sci U S A **105:**14603–14608. http://dx.doi.org/10.1073/pnas.0804138105.

24. **Weart RB, Levin PA**. 2003. Growth rate-dependent regulation of medial FtsZ ring formation. J Bacteriol **185:**2826–2834. http://dx.doi.org/10.1128/JB.185.9.2826-2834.2003.

25. **Kaltschmidt E, Wittmann HG**. 1970. Ribosomal proteins. XII. Number of proteins in small and large ribosomal subunits of *Escherichia coli* as determined by two-dimensional gel electrophoresis. Proc Natl Acad Sci U S A **67:**1276–1282. http://dx.doi.org/10.1073/pnas.67.3.1276.

26. **Rosenberg A, Sinai L, Smith Y, Ben-Yehuda S**. 2012. Dynamic expression of the translational machinery during *Bacillus subtilis* life cycle at a single cell level. PLoS One **7:**e41921. http://dx.doi.org/10.1371/journal.pone.0041921.

27. **Glaser P, Sharpe ME, Raether B, Perego M, Ohlsen K, Errington J**. 1997. Dynamic, mitotic-like behavior of a bacterial protein required for accurate chromosome partitioning. Genes Dev **11:**1160–1168. http://dx.doi.org/10.1101/gad.11.9.1160.

28. **Ireton K, Gunther NW, Grossman AD**. 1994. *spo0J* is required for normal chromosome segregation as well as the initiation of sporulation in *Bacillus subtilis*. J Bacteriol **176:**5320–5329.

29. **Lin DC, Grossman AD**. 1998. Identification and characterization of a bacterial chromosome partitioning site. Cell **92:**675–685. http://dx.doi.org/10.1016/S0092-8674(00)81135-6.

30. **Reizer J, Bachem S, Reizer A, Arnaud M, Saier MH, Jr, Stülke J**. 1999. Novel phosphotransferase system genes revealed by genome analysis—the complete complement of PTS proteins encoded within the genome of *Bacillus subtilis*. Microbiology **145:**3419–3429.

31. **Bi EF, Lutkenhaus J**. 1991. FtsZ ring structure associated with division in *Escherichia coli*. Nature **354:**161–164. http://dx.doi.org/10.1038/354161a0.

32. **Lutkenhaus J, Addinall SG**. 1997. Bacterial cell division and the Z ring. Annu Rev Biochem **66:**93–116. http://dx.doi.org/10.1146/annurev.biochem.66.1.93.

33. **Lonetto M, Gribskov M, Gross CA**. 1992. The sigma 70 family: sequence conservation and evolutionary relationships. J Bacteriol **174:**3843–3849.

34. **Wösten MM**. 1998. Eubacterial sigma-factors. FEMS Microbiol Rev **22:**127–150. http://dx.doi.org/10.1016/S0168-6445(98)00011-4.

35. **Lewis PJ, Errington J**. 1997. Direct evidence for active segregation of *oriC* regions of the *Bacillus subtilis* chromosome and co-localization with the Spo0J partitioning protein. Mol Microbiol **25:**945–954. http://dx.doi.org/10.1111/j.1365-2958.1997.mmi530.x.

36. **Lin DC, Levin PA, Grossman AD**. 1997. Bipolar localization of a chromosome partition protein in *Bacillus subtilis*. Proc Natl Acad Sci U S A **94:**4721–4726. http://dx.doi.org/10.1073/pnas.94.9.4721.

37. **Mascarenhas J, Weber MH, Graumann PL**. 2001. Specific polar localization of ribosomes in *Bacillus subtilis* depends on active transcription. EMBO Rep **2:**685–689. http://dx.doi.org/10.1093/embo-reports/kve160.

38. **Moriya S, Rashid RA, Rodrigues CD, Harry EJ**. 2010. Influence of the nucleoid and the early stages of DNA replication on positioning the division site in *Bacillus subtilis*. Mol Microbiol **76:**634–647. http://dx.doi.org/10.1111/j.1365-2958.2010.07102.x.

39. **Rodrigues CD, Harry EJ**. 2012. The Min system and nucleoid occlusion are not required for identifying the division site in *Bacillus subtilis* but ensure its efficient utilization. PLoS Genet **8:**e1002561. http://dx.doi.org/10.1371/journal.pgen.1002561.

40. **Pazos M, Casanova M, Palacios P, Margolin W, Natale P, Vicente M**. 2014. FtsZ placement in nucleoid-free bacteria. PLoS One **9:**e91984. http://dx.doi.org/10.1371/journal.pone.0091984.

41. **Sun Q, Yu XC, Margolin W**. 1998. Assembly of the FtsZ ring at the central division site in the absence of the chromosome. Mol Microbiol **29:**491–503. http://dx.doi.org/10.1046/j.1365-2958.1998.00942.x.

42. **Osawa M, Anderson DE, Erickson HP**. 2008. Reconstitution of contractile FtsZ rings in liposomes. Science **320:**792–794. http://dx.doi.org/10.1126/science.1154520.

43. **Baker TA, Sauer RT**. 2012. ClpXP, an ATP-powered unfolding and protein-degradation machine. Biochim Biophys Acta **1823:**15–28. http://dx.doi.org/10.1016/j.bbamcr.2011.06.007.

44. **Gottesman S**. 1999. Regulation by proteolysis: developmental switches. Curr Opin Microbiol **2:**142–147. http://dx.doi.org/10.1016/S1369-5274(99)80025-3.

45. **Jenal U, Hengge-Aronis R**. 2003. Regulation by proteolysis in bacterial cells. Curr Opin Microbiol **6:**163–172. http://dx.doi.org/10.1016/S1369-5274(03)00029-8.

46. **Lehnik-Habrink M, Lewis RJ, Mäder U, Stülke J**. 2012. RNA degradation in *Bacillus subtilis*: an interplay of essential endo- and exoribonucleases. Mol Microbiol **84:**1005–1017. http://dx.doi.org/10.1111/j.1365-2958.2012.08072.x.

47. **Bayles KW**. 2014. Bacterial programmed cell death: making sense of a paradox. Nat Rev Microbiol **12:**63–69. http://dx.doi.org/10.1038/nrmicro3136.

48. **Aizenman E, Engelberg-Kulka H, Glaser G**. 1996. An *Escherichia coli* chromosomal "addiction module" regulated by guanosine [corrected] 3′,5′-bispyrophosphate: a model for programmed bacterial cell death. Proc Natl Acad Sci U S A **93:**6059–6063. http://dx.doi.org/10.1073/pnas.93.12.6059.

49. **Bos J, Yakhnina AA, Gitai Z**. 2012. BapE DNA endonuclease induces an apoptotic-like response to DNA damage in *Caulobacter*. Proc Natl Acad Sci U S A **109:**18096–18101. http://dx.doi.org/10.1073/pnas.1213332109.

50. **Dwyer DJ, Camacho DM, Kohanski MA, Callura JM, Collins JJ**. 2012. Antibiotic-induced bacterial cell death exhibits physiological and biochemical hallmarks of apoptosis. Mol Cell **46:**561–572. http://dx.doi.org/10.1016/j.molcel.2012.04.027.

51. **Erental A, Sharon I, Engelberg-Kulka H**. 2012. Two programmed cell death systems in *Escherichia coli*: an apoptotic-like death is inhibited by the *mazEF*-mediated death pathway. PLoS Biol **10:**e1001281. http://dx.doi.org/10.1371/journal.pbio.1001281.

52. **Drlica K, Malik M, Kerns RJ, Zhao X**. 2008. Quinolone-mediated bacterial death. Antimicrob Agents Chemother **52:**385–392. http://dx.doi.org/10.1128/AAC.01617-06.

53. **Leytin V**. 2012. Apoptosis in the anucleate platelet. Blood Rev **26:**51–63. http://dx.doi.org/10.1016/j.blre.2011.10.002.

54. **Gibson DG, Glass JI, Lartigue C, Noskov VN, Chuang RY, Algire MA, Benders GA, Montague MG, Ma L, Moodie MM, Merryman C, Vashee S, Krishnakumar R, Assad-Garcia N, Andrews-Pfannkoch C, Denisova EA, Young L, Qi ZQ, Segall-Shapiro TH, Calvey CH, Parmar PP, Hutchison CA, III, Smith HO, Venter JC**. 2010. Creation of a bacterial cell controlled by a chemically synthesized genome. Science **329:**52–56. http://dx.doi.org/10.1126/science.1190719.

55. **Harwood C, Cutting SM**. 1990. Molecular biological methods for *Bacillus*. Wiley, Chichester, United Kingdom.

56. **Schaller A, Sun Z, Yang Y, Somoskovi A, Zhang Y**. 2002. Salicylate reduces susceptibility of *Mycobacterium tuberculosis* to multiple antituberculosis drugs. Antimicrob Agents Chemother **46:**2636–2639. http://dx.doi.org/10.1128/AAC.46.8.2636-2639.2002.